Zhenrong Li*, Chunlei Ma, Sugui Tian, Liqing Chen and Xianghua Liu

# Microstructure and Creep Property of Isothermal Forging GH4169G Superalloy

**Abstract:** By means of direct aging, microstructure observation and creep property measurement, the microstructure and creep behaviors of GH4169G superalloy are investigated. Results show that, after direct aging, the grain size is inhomogeneous in the alloy, and some δ precipitates discontinuously distribute in the grain and along the boundaries, which may improve the bonding strength of the boundaries. Under the experimental conditions, the creep activation energy of the alloy during steady-state creep are calculated to be Q = 594.7 kJ/mol. During creep, the deformation features of the alloy are twinning deformation and dislocations slipping in the matrix. As creep goes on, deformed dislocations pile up near the boundary regions to induce stress concentration for promoting the initiation and propagation of cracks along boundaries.

**Keywords:** GH4169G superalloy, microstructure, creep behavior

**PACS® (2010).** 81.40.Lm

***Corresponding author: Zhenrong Li:** College of Light Industry, Liaoning University, Shenyang 110036, China.
E-mail: lzr621206@126.com
**Chunlei Ma:** College of Light Industry, Liaoning University, Shenyang 110036, China
**Sugui Tian:** School of Materials Science and Engineering, Shenyang University of Technology, Shenyang 110870, China
**Liqing Chen, Xianghua Liu:** State Key Laboratory of Rolling and Automation, Northeastern University, Shenyang 110004, China

## 1 Introduction

Isothermal forging (ITF) GH4169G superalloy is a new alloy for adding trace elements of phosphorus and boron into GH4169 alloy [1, 2], and the microstructure of GH4169G alloy consists of γ matrix, γ′ and γ′′ phases [3]. Due to GH4169G alloy possessing good anti-fatigue, anti-oxidation and hot workability, the alloy is widely used to produce structural components of aero-engine, such as compressor shaft and turbine disk [4, 5].

Some researches [6, 7] have shown that, after adding trace elements of phosphorus and boron, the mechanical property and creep resistance of the alloy can be improved due to interaction of phosphorus and boron. Especially, the segregation of phosphorus and boron in the grain boundaries may cause granular phase precipitating along boundaries, which may restrain boundary slipping and enhance boundary strength to improve creep resistance of the alloy [8, 9]. When phosphorus and boron segregated in the grain, the Suzuki effect induced near the dislocations may hinder the dislocation movement to decrease the strain rate of the alloy during steady state creep [10, 11]. Researches [12, 13] have shown that deformation feature of GH4169 alloy is twinning deformation, but creep behavior of GH4169G alloy is still not clear.

In this paper, ITF-GH4169G superalloy is direct aged, and then creep property of the alloy is measured under experimental conditions, and the microstructures of the alloy is observed by scanning electron microscopy (SEM) and transmission electron microscopy (TEM) to investigate the microstructure and creep behaviors of GH4169G alloy.

## 2 Experimental

The GH4169G alloy is smelted in the vacuum induction furnace and poured into ingot, and then the ingot is prepared into square billet by isothermal forging. Here, the initial forging temperature is 1100 °C, and final forging temperature is 950 °C, and then cooling in the air. After the alloy is prepared by ITF process, the alloy is kept at 720 °C for 8 h, and is cooled to 620 °C in the rate of 50 °C/h in the furnace, and then is kept at 620 °C for 8 h. After that the alloy is cooled in the air. The heat treatment mentioned above is defined as direct aging treatment (DAT). And the error range of heat treatment furnace is ±5 °C. The chemical composition of GH4169G alloy is shown in Table 1.

After direct aging, the ingot of the ITF-GH4169 alloy is cut into the specimens with the cross-section of 4.5 mm × 2.5 mm and the gauge length of 19 mm. Uniaxial constant load tensile testing was performed, in a GWT504-model creep testing machine, for measuring creep curves under the experimental conditions (650~670 °C and 700~750 MPa). By TEM the microstructures of the alloy are

**Table 1:** Chemical composition of GH4169G alloy (mass fraction, %)

| Cr | Al | Ti | Mo | Nb+Ta | Co | P | B | Ni | Fe |
|---|---|---|---|---|---|---|---|---|---|
| 19 | 0.6 | 1.2 | 3.0 | 5.1 | ≤1.0 | 0.022 | 0.005 | 53 | Bal. |

observed to investigate the microstructure and deformation mechanism of the alloy.

# 3 Results

## 3.1 Microstructure of GH4169G superalloy

After direct aging, the microstructure of GH4169G superalloy is shown in Fig. 1, indicating that grain size of the alloy is about 5~12 μm. The twinning appears in the grain as marked by the long arrow in Fig. 1, and some white granular phase precipitates in the grain and along boundaries, as marked by the short arrows in Fig. 1.

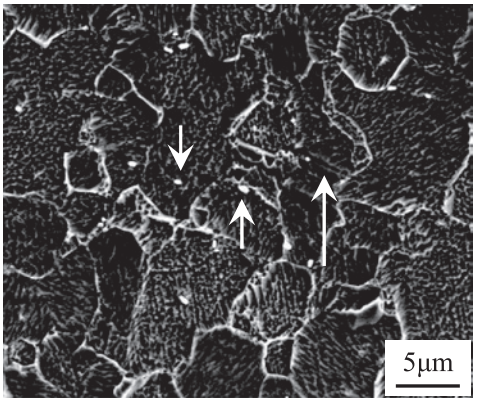


**Fig. 1:** Microstructure of the isothermal forged GH4169G superalloy

The TEM microstructures of GH4169G alloy are shown in Fig. 2. The microstructure of γ′ phase and γ″ phase in the matrix is shown in Fig. 2(a), thereinto, the γ′ phase display spheroid as marked by the white arrow, and the flat-ellipsoidal γ″ phase is marked by the black arrow in Fig. 2(a). Besides, the microstructure of twinning is marked by the long arrow as shown in Fig. 2(b), and the granular precipitates dispersedly distribute in the alloy as marked by the short arrows. By means of transmission electron microscopy (TEM) and energy dispersion spectrum (EDS), it is detected that the elements of Nb and Ni are richer in the phase. Besides, the corresponding selected area electron diffraction (SAED) and index determination are shown in Fig. 2(c), which can determine the phase is $Ni_3Nb$-δ phase.

## 3.2 Creep property of GH4169G superalloy

After direct aging, the creep curves of ITF-GH4169G superalloy measured under different experimental conditions are shown in Fig. 3. Under the conditions of applied stress of 700 MPa at different temperatures, the creep curves of the alloy are shown in Fig. 3(a). When the applied temperature is 650 °C, the alloy possesses smaller strain rate (0.0022%/h) during steady state creep and longer creep lifetime (362 h), and its elongation is about 11.2%. As the applied temperature increases to 660 °C, the steady strain rate enhances to 0.0050%/h, and its duration is measured to be 200 h during steady state creep, and the creep lifetime of the alloy decreases to 271 h. As the temperature further increases to 670 °C, the creep lifetime of the alloy

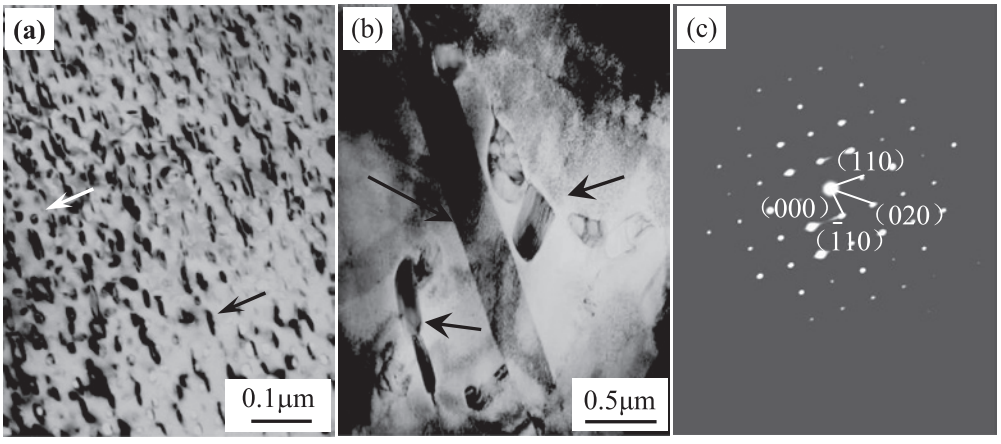


**Fig. 2:** Morphology of isothermal forged GH4169G alloy after direct aging. (a) γ′ phase and γ″ phase in the matrix, (b) δ phase and twinning in the alloy, (c) SAED of δ phase

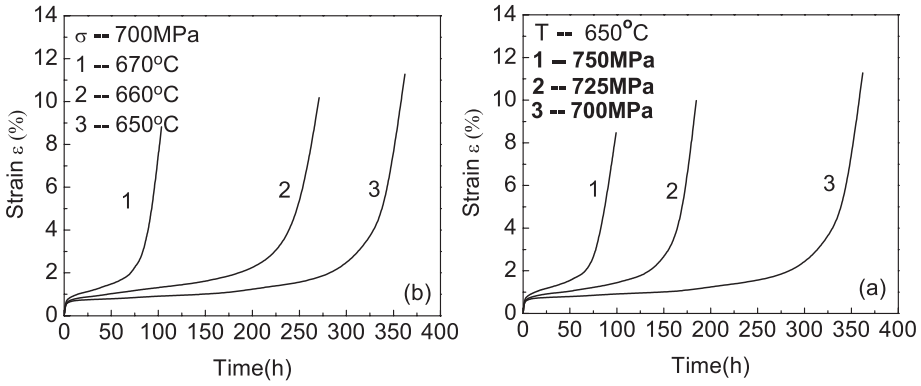


**Fig. 3:** Creep curves of ITF-DA GH4169G alloy in different conditions. (a) Various temperatures, (b) various stresses

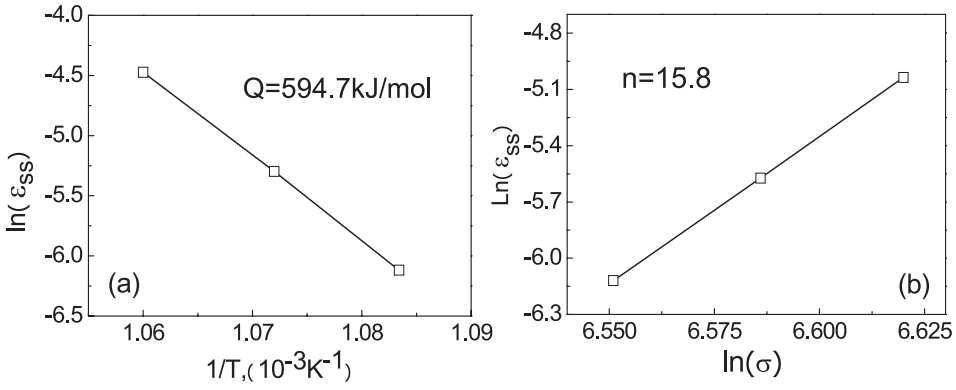


**Fig. 4:** Relationship between the strain rate and the applied temperatures, stresses during the steady state creep. (a) Relationship between the strain rate and temperature, (b) relationship between the strain rate and the applied stresses

decreases to 103 h. The fact mentioned above indicates that GH4169G alloy is sensitive to the applied temperature obviously.

Under the conditions of applied different stresses at 650 °C, the creep curves of the alloy are shown in Fig. 3(b). When the applied stresses are 725 MPa and 750 MPa, the strain rates of the alloy are measured to be 0.0038%/h and 0.0065%/h during steady state creep, respectively. And the creep lifetimes of the alloy decrease to 184 h and 99 h with the applied stress enhancing, respectively.

The steady-state strain rates of the alloys obey Dorn law during steady creep state, and its formula can be expressed as follows:

$$\dot{\varepsilon} = A\sigma^n \exp(\frac{-Q_a}{RT}) \quad (1)$$

where $\dot{\varepsilon}$ is the steady-state strain rate, $A$ is a constant, $\sigma$ is the applied stress, $T$ is the temperature, and $Q_a$ is the apparent creep activation energy.

The steady-state strain rate of GH4169G alloy can be measured under experimental conditions of 650~670 °C and 700~750 MPa. According to the relationship between steady-state strain rates and applied temperatures, the apparent creep activation energy of the alloy is measured to be Q = 594.7 kJ/mol, as shown in Fig. 4(a). Fig. 4(b) shows the relationship between steady-state strain rates and the applied stresses, and the stress exponent of the alloy is measured to be n = 15.8.

## 3.3 Deformation features of GH4169G alloy during creep

Under the conditions of 650 °C and 700 MPa, the microstructures of ITF-GH4169G alloy crept for 362 h up to fracture are shown in Fig. 5. In local region of fracture alloy, the grain boundary of the alloy is marked by the black long arrow in Fig. 5(a), and some δ phase discontinuously precipitate along the boundaries as marked by the black short arrow. Slipping dislocations pile up near the δ phase as marked by letter A, which indicates that the δ phase precipitated along boundaries may effectively hinder dislocation movement. In the right side of the boundary, a

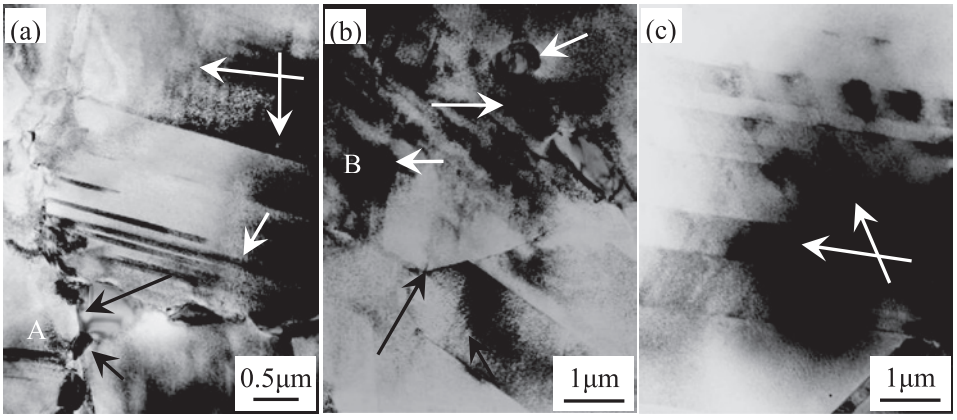


**Fig. 5:** Microstructure of the direct aged ITF-GH4169G alloy crept for 362 h up to fracture at 650 °C/700 Mpa. (a) δ-particles distribute along the boundary, and the dislocations tangles up as marked with letter A, (b) dislocations tangle up around the δ particles as marked with letter B, (c) twinning with different orientations in the alloy

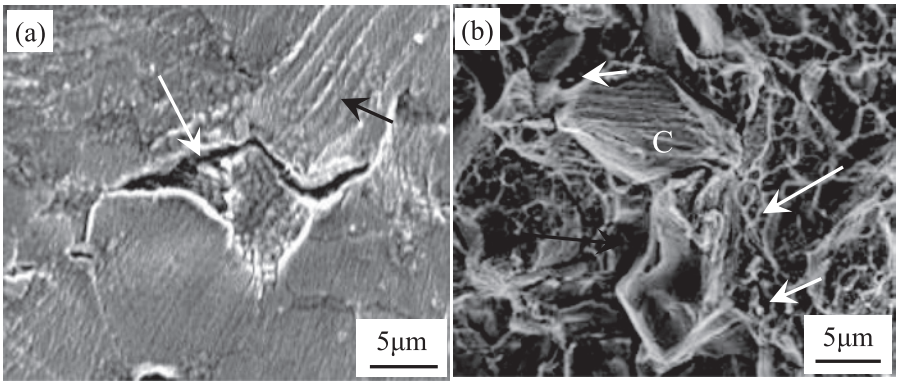


**Fig. 6:** Fracture morphology of the ITF-GH4169G alloy crept for 362 h up to fracture at 650 °C/700 MPa. (a) Fracture feature along the boundary, (b) fracture morphology

group of deformation twinning appears in the matrix as marked by the short white arrow, and the twinning ends at the grain boundary. Besides, slipping dislocations with double orientations appear on the top of twinning boundary as marked by the crossed arrows.

In another local region of the fracture alloy, granular δ phase precipitated in the grain are marked by the short white arrows in Fig. 5(b). As creep goes on, deformed twinning with parallel feature form in the matrix, and part of twinning ending at the δ phase is marked by the white long arrow. Besides, deformed dislocations tangle up around δ phase as marked by letter B. The fact mentioned above indicates that the δ phase precipitated in the matrix may hinder the twinning deformation and dislocation movement to enhance the creep resistance of the alloy. Beneath the grain boundary as marked by the black long arrow, high density of slipping dislocations appear in the twinning, as marked the black short arrow in Fig. 5(b). Fig. 5(c) shows that deformed twinning with different orientations marked with the crossed arrows exist in the matrix of the alloy, which can coordinate the grain deformation during creep.

After GH4169G alloy crept to fracture under the conditions of 650 °C and 700 MPa, the fracture morphology of the alloy is shown in Fig. 6. Slipping traces on surface of the fracture alloy are marked by the black arrow in Fig. 6(a), and the cracks propagate along the grain boundaries, and the δ particle remains in the fracture as marked by the white arrow, which result in the fracture possessing unsmooth feature. The fact mentioned above indicates that the δ phase precipitated along boundary may hinder the boundary slide to enhance the creep resistance of the alloy. The fracture morphology of the alloy is shown in Fig. 6(b), which indicates that the alloy possesses the feature of intergranular fracture as marked by the black long arrow. And some δ particles remain in the fracture as marked by the short white arrows. Besides the dissociation plane with some slipping traces appears in the frac-

ture as marked by letter C. In the left side of the dissociation plane, shallow dimples appear in the fracture, as marked by the white long arrow in Fig. 6(b).

## 4 Discussion

After direct aging, some granular δ phase precipitated in the grain and along boundaries of GH4169G alloy. And the fact of δ particles distributing along boundary may enhance the boundary strength to hinder the boundary slide during creep.

During creep, the deformation features of GH4169G alloy are the twinning deformation and dislocations with double orientations slipping in the matrix. Thereinto, slipping dislocations with double orientations activated in the matrix may release the stress concentration induced by the fact of dislocations piling up near the boundaries, which can delay the crack initiation along the boundaries. Besides the δ phase precipitated along the boundary can effectively restrain the dislocation movement to enhance the creep resistance of the alloy. The facts mentioned above are the main reasons for the alloy possessing good creep property.

Compared with GH4169G alloy, the fracture of GH4169 alloy crept up to rupture possesses smooth feature due to the fact that no granular phase precipitates along the boundaries [14]. As creep goes on, deformed dislocations are activated in the matrix, and the slipping dislocations pile up near the boundaries and tangle up around δ phase. And the amount of dislocations piled up around the boundaries increases to bring out the stress concentration. When the value of stress concentration exceeds the yield strength of the alloy, the cracks may initiate and propagate along the grain boundaries. Although δ particles precipitated along boundaries can restrain the boundary slide to enhance the boundary strength, the fact of cracks still initiating and propagating along boundary indicates that the grain boundaries are the weakness of the alloy during creep.

## 5 Conclusions

1. After direct aging, the microstructure of ITF-GH4169G alloy consists of $\gamma'$ , $\gamma''$ and δ phases, and the gain size is inhomogeneous, and the δ phase precipitated along boundary may enhance the boundary strength to enhance the creep resistance of the alloy.
2. During creep, the deformation mechanisms of GH4169G alloy are that twinning deformation and deformed dislocations with double orientations slipping in the matrix. As creep goes on, slipping dislocations pile up near the boundaries to cause the stress concentration for the cracks initiating and propagating along boundaries, which is thought to be the fracture mechanism of the alloy.

Received: July 7, 2013. Accepted: November 15, 2013.

## References

[1] J. M. Zhang, Z. Y. Gao, J. Y. Zhuang, et al. *Metall. Mater. Trans. A*, 30(1999) 2701–2712.
[2] G. F. Lovicu, C. Colombo, M. D. Sanctis, et al. *Metall. Mater. Trans. A*, 42(2011) 3577–3580.
[3] F. Klocke, V. Backer, H. Wegner, et al. *Metall. Mater. Trans. A*, 3(2009) 391–399.
[4] O. Roder, J. Albrecht, G. Lutjering. *Mater. High Temp.*, 23(2006) 171–177.
[5] Z. Q. Hu, W. R. Sun, S. R. Guo. *Acta Metall. Sin., (English letters)*, 9(1996) 443–452.
[6] D. H. Kim, J. H. Kim, J. W. Sa, et al. *Mater. Sci. Eng. A*, 483–484(2008): 262–265.
[7] D. Dye, O. Hunziker, S. M. Roberts, et al. *Metall. Mater. Trans. A*, 32(2001) 1713–1725.
[8] T. Antonsson, H. Fredriksson. *Metall. Mater. Trans. B*, 36(2005) 85–96.
[9] P. D. Hicks, C. J. Attstetter. *Metall. Mater. Trans. A*, 23(1992) 237–249.
[10] C. G. Mckamey, C. A. Carmichael, W. D. Cao, et al. *Scripta Mater.,* 38(1998) 485–491.
[11] Z. J. Miao, A. D. Shan, Y. B. Wu, et al. *T. Nonferr. Metal. Soc.*, 22(2012) 318–323.
[12] X. Huang, M. C. Chaturved, N. L. Richards, et al. *Acta Mater.,* 45(1997) 3095–3107.
[13] Y. Q. Ning, M. W. Fu, X. Chen. *Mater. Sci. Eng. A,* 540(2012) 164–173.
[14] S. G. Tian, Z. R. Li, Z. G. Zhao, et al. *Mater. Sci. Eng. A,* 550(2012) 235–242.